Revision 2 of ms: 5481

Dislocation microstructures in simple-shear-deformed wadsleyite at transition-zone conditions: Weak-beam dark-field TEM characterization of dislocations on the (010) plane.

Nobuyoshi Miyajima* and Takaaki Kawazoe

Bayerisches Geoinstitut, Universität Bayreuth, D-95440 Bayreuth, Germany

* Corresponding author:

e-mail address: Nobuyoshi.Miyajima@uni-bayreuth.de

ABSTRACT

Dislocation microstructures of an (010)[001]-textured wadsleyite have been investigated in weak-beam dark-field imaging in a transmission electron microscope. 1/2<101> partial dislocations on the (010) plane are characterized with [100] dislocations on the (001) plane and 1/2<111> dislocations forming {011} slip bands. The partial dislocations are extended on the (010) stacking fault as a glide configuration (i.e., Shockley-type stacking faults with 1/2<101> displacement vector). The [001] slip on the (010) plane occurs by glide of the dissociated dislocations, which can play an important role in the generation of the crystallographic preferred-orientation patterns reported in water-poor deformation conditions. The glide mechanism on the (010) plane leave the oxygen sub-lattice unaffected, but changes the cation distribution, forming a defective stacking sequence of the magnesium cations in the process of dislocation gliding. The mechanism might be related to transformation plasticity and related effects, such as transformation-enhanced weakening and deep-focus earthquakes in the mantle transition zone.

Keywords: *wadsleyite, slip systems, slip plane, Burgers vector, Shockley-type extended dislocation, Frank's rule, Chalmers-Martius criterion*

INTRODUCTION

Enigmatic [001] glide on the (010) plane; i.e., the [001](010) slip system, in deformed wadsleyite has been recently deduced from crystallographic preferred orientation (CPO) patterns obtained by deformation experiments (Demouchy et al. 2011; Kawazoe et al. 2013; Ohuchi et al. 2014). In their studies, wadsleyite aggregate was deformed at pressure-temperature conditions characteristic of the mantle transition zone, and a [001](010)-textured CPO pattern was found from electron backscatter diffraction (EBSD) measurement on recovered samples. The CPO pattern is primarily controlled by the easiest slip system. In the case of olivine, a polymorph of wadsleyite, deformation fabrics are well correlated with the dominant slip systems (Karato et al. 2008). Therefore, activation of the [001](010) slip system is simply expected in deformed wadsleyite. Identification of the easiest slip system in wadsleyite is important in understanding the physical mechanisms of its plastic deformation (Tommasi et al. 2004) and, in turn, for interpretation of seismic anisotropy observed in the mantle transition zone (Foley and Long 2011; Yuan and Beghein 2013).

However, real activation of the [001](010) slip system has not yet been confirmed clearly by dislocation microstructures in conventional bright-field and dark-field transmission electron microscopy (TEM) (Cordier 2002). TEM observations in the early 1980s were made on wadsleyite that had been naturally deformed in shocked meteorites (Price et al. 1982; Madon and Poirier 1983; Price 1983). The (010) stacking faults were found in the deformed wadsleyite, and a topotaxial transformation from ringwoodite to wadsleyite was suggested to occur by a martensitic shear mechanism. In addition, wadsleyite was experimentally deformed in a Kawai-type multianvil apparatus (Sharp et al. 1994; Thurel and Cordier 2003a; Thurel et al. 2003b). Subsequent TEM characterization of recovered samples revealed activation of the following slip systems: [100](010), [100](001), [100]{011}, [100]{021}, 1/2<111>{101}, [010](001), [010]{101} and <101>(010). Wadsleyite was also deformed at 14-20 GPa and 1690-2100 K using a rotational Drickamer apparatus (Hustoft et al. 2013; Kawazoe et al. 2010a; Farla et al. 2015). However, the [001](010) slip system could not be determined by TEM because the dislocation density was too high to apply the invisibility criterion using conventional bright and dark field TEM imaging.

The (010) stacking fault is a characteristic microstructure in deformed wadsleyite having the (010)[001]-textured CPO (Demouchy et al. 2011; Ohuchi et al. 2014). Previous studies have discussed that Shockley-type (010) stacking faults can be formed through the glide of 1/2<101> partial dislocations on the (010) plane (e.g., Price 1983; Sharp et al. 1994). Based on their theoretical study on crystal chemistry and anisotropic linear elasticity of wadsleyite, Thurel et al. (2003c) reported a possible dissociation along [001] = 1/2[-101] + 1/2[101]. They recommended further detailed investigation on the precise core structure of the dislocations in wadsleyite to better understand and model the plastic behavior of wadsleyite. In this context, Metsue et al. (2010) concluded that, from their calculation of the generalized stacking faults energies on the (010) plane, [001] shear is only possible in (010) where the dislocations dissociate into two non-collinear partial dislocations of ***b*** = 1/2<101>, i.e., 1/2[-101] and 1/2[101]. Also, as mentioned in Demouchy et al. (2011), viscoplastic self-consistent (VPSC) modeling of CPO evolution using the previously reported glide systems for wadsleyite, i.e., [100]{0kl} and 1/2<111>{101}, cannot reproduce the measured CPO pattern, unless the [001](010) system is also activated. However, they could not confirm such dislocations by TEM. Therefore, we have re-examined a deformed wadsleyite with the [001](010) fabric by using weak-beam dark-field (WBDF) TEM imaging.

EXPERIMENTAL METHOD

Deformation experiment

The simple-shear deformation experiment on a wadsleyite aggregate was performed to a strain *γ* of 0.4 at a strain rate of 3 × 10^{-5} s^{-1} at 18 GPa and 1800 K with a deformation-DIA apparatus (run M0180 in Kawazoe et al. 2013). Tungsten carbide anvils with a 3-mm truncation were adopted to reach the target pressure (Kawazoe et al., 2010b). The starting material was a single crystal of San Carlos olivine that had been transformed to polycrystalline wadsleyite at 18 GPa and high temperature. Grain size and water content of a recovered sample were evaluated as 2.8 μm and 134 wt ppm H_2O, respectively. Further experimental details of the experiment were described in Kawazoe et al. (2013). For comparison, an undeformed wadsleyite (run M0187) in the same series experiment was also observed.

TEM sample and the procedure of the sample preparation

The recovered wadsleyite sample from the deformation experiment was Ar-ion milled to electron transparency at an accelerating voltage of 6 kV and then finally thinned at 2–4 kV with an incident angle of 4-5 degree using an ion slicer (JEOL EM-09100IS) and coated with amorphous carbon for transmission electron microscopy. WBDF-TEM imaging was performed in a field emission transmission electron microscope, Philips CM20FEG, operated at 200 kV. The WBDF-

TEM images are recorded by using slow-scan CCD camera (Gatan 698) and KODAK SO-160 TEM negative films.

The Burgers vectors of the dislocations were characterized based on the conventional invisibility criterion method: **g.b** = 0 and **g**.(**b** × **u**) = 0, where **g**, **b** and **u** are the diffraction vector, the Burgers vector, and the unit vector along the dislocation line, respectively. In addition, the thickness contour fringe method (Ishida et al. 1980; Miyajima and Walte 2009) was used for confirmation of a particular Burgers vector, e.g. 1/2<101>, from possible candidates by constraining the magnitude of the Burgers vector. The number *n* of terminating thickness contour fringes at the extremity of a free dislocation was counted in the WBDF images and applied to the relation **g**.**b** = *n*.

TEM OBSERVATION AND THE RESULTS

The typical dislocation structures are displayed in Figure 1. The long screw segment of [100] dislocations are visible in a WBDF TEM image along the [001] zone axis direction, which is likely to indicate a strong lattice friction (see detail in the discussion) along the [100] zone axis and less mobility of the screw segment than the edge one (Thurel and Cordier 2003). A few orthogonal dislocation lines belong to 1/2<111> type dislocations (Fig. 1a). In the other grain observed along the [100] zone axis, the dislocation arrays, i.e. slip bands, are parallel to the projection of the (0-11) plane and consist of 1/2<111> perfect dislocations that have dissociated into some partial dislocations at the tens of nanometer scale (Fig. 1b). The configuration of the dislocation bands is consistent with the 1/2<111>{101} slip system.

One of the most important characters to explain the (010)[001] fabric is that a high density of dislocations parallel to both the [101] and [-101] directions are visible in WBDF images with **g** = 400 and **g** = 004, while one of those two dislocations is invisible systematically with **g** = 404 and -404, respectively observed along the [010] zone axis (Fig. 2 and S1). The dislocation lines are also most likely to be on the (010) plane, not on the {101} planes, because of their long projection lengths on the plane and because no oscillation contrast exists along the lines which indicate that the dislocation lines are not strongly inclined in the [010]-oriented TEM foil (about 200 nm thickness on the middle of the image) but almost parallel to the foil. Also, two thickness contour fringes are terminated at the extremity of the dislocation in the WBDF images with **g** = 004 (indicated by white arrowheads in Fig. 3). From the number (*n*) of terminating thickness fringes at the extremity of a dislocation from a wedge-shaped thin-foil specimen (Ishida et al. 1980; Miyajima and Walte 2009), we can determine that its vector product of $\mathbf{g}_{004}$ and the Burgers vector, **b** of the dislocations is two, consistent with **b** = 1/2 [*uv*1].

Moreover, WBDF-TEM images with diffraction vectors, **g** = -211 and **g** = 013, i.e. two independent diffraction vectors to the (010) plane, display Shockley-type extended dislocations with **b** = 1/2 <101> on the end of their associated stacking faults with fringe contrast on the (010) plane along the [101] direction (Fig. 4 and S2). The stacking fault energy of the (010) stacking fault is likely to be low because of the wide distance between partial dislocations.

From all the results obtained from the WBDF images, we conclude that [001] dislocations in the deformed wadsleyite are dissociated to a pair of screw-character 1/2<101> dislocations on the (010) plane; i.e. **b** = 1/2[101] and **b** = 1/2[-101]:

The partial dislocations glide in the (010) plane.

For comparison, typical microstructures of the (010) stacking fault in an undeformed sample (M0187 in Kawazoe eta l. 2013) are also shown in the WBDF images with **g** = -2-1-1 and 0-80 (Fig. 5). Stacking faults with partial dislocations at the ends are not well aligned along a potential macroscopic strain direction, and a number of ledges exist on the stacking faults (Fig. S4, Supplementary Material). The microstructures are in contrast to a glide configuration in Figure 4b. The density of stacking faults in individual grains is also much less than that of deformed sample, M0180 (Figs. 4b and S3) and most grains do not contain stacking faults and dislocations (e.g., Fig. 4d in Kawazoe et al. 2013).

DISCUSSION

A [001] slip on the (010) plane has previously been predicted from the enigmatic CPO pattern in deformed wadsleyite. In this study, we have intensively studied wadsleyite grains along the [010] and [100] zone axes, from which we could directly investigate the <*u*0*w*> and <0*vw*> type dislocations on the (010) plane and the (100) plane, respectively. In the WBDF-TEM images, a high density of 1/2<101> partial screw dislocations and screw-dominant [100] dislocations are co-activated on the (010) plane (Figs. 2, 3 and S1). Herein we confirmed that a pair of partial dislocations with Shockley-type stacking fault on the (010) plane are a glide configuration, which can contribute bulk strain in the simple-shear deformation and result in the development of the (010)[001]-textured CPO pattern in wadsleyite. The configurations of the straight dislocation lines of both dislocations with **b** = 1/2<101> and [100] also indicate a high Peierls stress, lying in potential valleys on the slip planes (Poirier 2000). Note that co-activation of the (010)[100] slip system cannot be neglected, wadsleyite CPO was affected and thus its pattern had slightly deviated from the ideal (010)[001]-textured CPO, with a small maximum of the [100] axis in the CPO pattern of the M0180 sample (Fig. 6a of Kawazoe et al. 2013).

The (010) stacking faults have been frequently observed in synthetic and natural wadsleyite from high pressure experiments and shocked meteorites (Madon and Poirier 1983;

Price 1983; Price et al. 1982), respectively. As well, some of wadsleyite grains in a non-deformed sample, M0187 in Kawazoe et al. (2013) display the stacking faults which are not a glide configuration. However, few previous studies on the wadsleyite have insisted on the potential of [001] slip by the glide of dissociated dislocations producing Shockley-type stacking faults on the basis of theoretical viewpoints of the *Frank Criterion* (e.g., Sharp et al. 1994) and of a dislocation core model based on the *Peierls–Nabarro–Galerkin* model (Metsue et al. 2010, also see Supplementary Material). As Demouchy et al. (2011) reported based on their VPSC approach, unless the [001](010) system is activated, contributions from only the previously reported [100]{0*kl*} and 1/2<111>{101} system cannot reproduce the unique CPO in which the [100] and [001] axes are preferentially sub-parallel to the shear direction and the [010] axes concentrate in the direction of the shear-plane normal (e.g., Fig. 10B in Demouchy et al. 2011). Therefore, the glide of 1/2<101> partial dislocations on the (010) plane, which were characterized in this study, is a major requisite for the deformation mechanisms in the (010)[001]-textured wadsleyite. The dissociation of a [001] perfect dislocation into two non-collinear partial dislocations of 1/2[-101] and 1/2[101] is consistent with their theoretical model by Metsue et al. 2010. The [001] slip on the (010) plane occurs by glide of the dissociated dislocations, which can reasonably explain the reported CPO pattern (Demouchy et al. 2011; Kawazoe et al. 2013; Ohuchi et al. 2014).

IMPLICATIONS

We clearly bridge a gap between the bulk fabric and dislocation microstructures in the deformed wadsleyite displaying the enigmatic (010)[001] fabric. The slip in the [001] direction on the (010) plane by the activation of 1/2<101> partial dislocations is likely to play an important role in the previous studies of deformed wadsleyite. The deformation mechanisms on the (010) plane of wadsleyite might be an alternative explanation of transformation-enhanced weakening (Price 1983) and deep-focus earthquake in the mantle transition zone (Rubie and Brearley 1994). ~~Just because~~, At the atomic scale, the stacking faults on the (010) plane is not due to a rearrangement on the closest packing plane of oxygens, i.e. {101} and {021} planes (Smyth et al. 2012), but due to a defective stacking sequence of the magnesium cations in the process of dislocation gliding (see Supplementary Material) and also during the olivine-wadsleyite transformation under a deviatric stress (Fujino and Irifune, 1992).

ACKNOWLEDGMENTS

We thank P. Cordier for constructive discussion on dislocation microstructures and providing a copy of Ph.D thesis of E. Thurel. Discussion with K. Fujino is also appreciated. Crystal structure was drawn with software VESTA in the Supplementary Material.

REFERENCES CITED

Cordier, P. (2002) Dislocations and slip systems of mantle minerals. In S. Karato, and H.-R. Wenk, Eds. Plastic Deformation of Minerals and Rocks, 51, 137-179. American Mineralogical Society, Washington DC.

Demouchy, S., Mainprice, D., Tommasi, A., Couvy, H., Barou, F., Frost, D.J., and Cordier, P. (2011) Forsterite to wadsleyite phase transformation under shear stress and consequences for the Earth's mantle transition zone. Physics of the Earth and Planetary Interiors, 184(1-2), 91-104.

Farla, R., Amulele, G., Girard, J., Miyajima, N., and Karato, S.i. (2015) High‐pressure and high-temperature deformation experiments on polycrystalline wadsleyite using the rotational Drickamer apparatus. Phys Chem Minerals, in press.

Foley, B.J., and Long, M.D. (2011) Upper and mid-mantle anisotropy beneath the Tonga slab. Geophysical Research Letters, 38.

Fujino, K., and Irifune, T. (1992) TEM Studies on the Olivine to Modified Spinel Transformation in Mg_2SiO_4. High-Pressure Research: Application to Earth and Planetary Sciences, Geophysical Monograph Series, 237-243.

Hustoft, J., Amulele, G., Ando, J., Otsuka, K., Du, Z.X., Jing, Z.C., and Karato, S.I. (2013) Plastic deformation experiments to high strain on mantle transition zone minerals wadsleyite and ringwoodite in the rotational Drickamer apparatus. Earth and Planetary Science Letters, 361, 7-15.

Ishida, Y., Ishida, H., Kohra, K., and Ichinose, H. (1980) Determination of the Burgers Vector of a Dislocation by Weak-Beam Imaging in a Hvem. Philosophical Magazine a-Physics of Condensed Matter Structure Defects and Mechanical Properties, 42(4), 453-462.

Karato, S., Jung, H., Katayama, I., and Skemer, P. (2008) Geodynamic significance of seismic anisotropy of the upper mantle: New insights from laboratory studies. Annual Review of Earth and Planetary Sciences, 36, 59-95.

Kawazoe, T., Karato, S., Ando, J., Jing, Z.C., Otsuka, K., and Hustoft, J.W. (2010) Shear deformation of polycrystalline wadsleyite up to 2100 K at 14-17 GPa using a rotational Drickamer apparatus (RDA). Journal of Geophysical Research-Solid Earth, 115.

Kawazoe, T., Nishiyama, N., Nishihara, Y., and Irifune, T. (2010) Deformation experiment at P-T conditions of the mantle transition zone using D-DIA apparatus. Physics of the Earth and Planetary Interiors, 183(1-2), 190-195.

(DOI will not work until issue is live.) DOI: http://dx.doi.org/10.2138/am-2015-5481

Kawazoe, T., Ohuchi, T., Nishihara, Y., Nishiyama, N., Fujino, K., and Irifune, T. (2013) Seismic anisotropy in the mantle transition zone induced by shear deformation of wadsleyite. Physics of the Earth and Planetary Interiors, 216, 91-98.

Madon, M., and Poirier, J.P. (1983) Transmission Electron-Microscope Observation of Alpha,Beta and Gamma $(Mg,Fe)_2SiO_4$ in Shocked Meteorites - Planar Defects and Polymorphic Transitions. Physics of the Earth and Planetary Interiors, 33(1), 31-44.

Metsue, A., Carrez, P., Denoual, C., Mainprice, D., and Cordier, P. (2010) Plastic deformation of wadsleyite: IV Dislocation core modelling based on the Peierls-Nabarro-Galerkin model. Acta Materialia, 58(5), 1467-1478.

Miyajima, N., and Walte, N. (2009) Burgers vector determination in deformed perovskite and post-perovskite of $CaIrO_3$ using thickness fringes in weak-beam dark-field images. Ultramicroscopy, 109(6), 683-692.

Ohuchi, T., Fujino, K., Kawazoe, T., and Irifune, T. (2014) Crystallographic preferred orientation of wadsleyite and ringwoodite: Effects of phase transformation and water on seismic anisotropy in the mantle transition zone. Earth and Planetary Science Letters, 397, 133-144.

Poirier, J.-P. (2000) Introduction to the Physics of the Earth's interior. 312 p. Cambridge University Press.

Price, G.D. (1983) The Nature and Significance of Stacking-Faults in Wadsleyite, Natural Beta-(Mg, Fe)2sio4 from the Peace River Meteorite. Physics of the Earth and Planetary Interiors, 33(2), 137-147.

Price, G.D., Putnis, A., and Smith, D.G.W. (1982) A Spinel to Beta-Phase Transformation Mechanism in (Mg,Fe)2sio4. Nature, 296(5859), 729-731.

Rubie, D.C., and Brearley, A.J. (1994) Phase-Transitions between Beta-$(Mg,Fe)_2SiO_4$ and Gamma-$(Mg,Fe)_2SiO_4$ in the Earth's Mantle - Mechanisms and Rheological Implications. Science, 264(5164), 1445-1448.

Sharp, T.G., Bussod, G.Y.A., and Katsura, T. (1994) Microstructures in Beta-$Mg_{1.8}Fe_{0.2}SiO_4$ Experimentally Deformed at Transition-Zone Conditions. Physics of the Earth and Planetary Interiors, 86(1-3), 69-83.

Smyth, J.R., Miyajima, N., Huss, G.R., Hellebrand, E., Rubie, D.C., and Frost, D.J. (2012) Olivine-wadsleyite-pyroxene topotaxy: Evidence for coherent nucleation and diffusion-controlled growth at the 410-km discontinuity. Physics of the Earth and Planetary Interiors, 200, 85-91.

Thurel, E., and Cordier, P. (2003) Plastic deformation of wadsleyite: I. High-pressure deformation in compression. Physics and Chemistry of Minerals, 30(5), 256-266.

Thurel, E., Cordier, P., Frost, D., and Karato, S.I. (2003) Plastic deformation of wadsleyite: II. High-pressure deformation in shear. Physics and Chemistry of Minerals, 30(5), 267-270.

Thurel, E., Douin, J., and Cordier, P. (2003) Plastic deformation of wadsleyite: III. Interpretation of dislocations and slip systems. Physics and Chemistry of Minerals, 30(5), 271-279.

Tommasi, A., Mainprice, D., Cordier, P., Thoraval, C., and Couvy, H. (2004) Strain-induced seismic anisotropy of wadsleyite polycrystals and flow patterns in the mantle transition zone. Journal of Geophysical Research-Solid Earth, 109(B12).

Yuan, K., and Beghein, C. (2013) Seismic anisotropy changes across upper mantle phase transitions. Earth and Planetary Science Letters, 374(0), 132-144.

FIGURE CAPTIONS

Figure 1. Typical dislocation microstructures of the simple-shear deformed wadsleyite (run M0180 in Kawazoe et al. 2013). (a) Straight, long screw segments of [100] dislocations (black arrowhead) and a few of 1/2[111] dislocations (Lower left, white arrowhead) are visible. (b) Array of 1/2[111] dislocations that have dissociated into several partial dislocations (black arrowheads) are in dislocation bands parallel to the (0-11) plane. The residual contrast of stacking faults on the (010) plane is weakly visible (white arrowheads). The stacking faults on the (010) plane are also indicated by remarkable streak lines along the [010]* direction on the selected area electron diffraction (SAED) pattern of the nearest zone axis (c). The two-sided arrows on the upper left and upper right in (a) and (b), respectively indicate approximately the bulk shear direction in the deformation experiment.

Figure 2. Typical WBDF images of 1/2 <101> dislocations co-activated with [100] dislocations. (a) A whole grain with **g** = 004, the inset is the nearest principal zone axis. The right half of the grain with (b) **g** = 400 (c) **g** = 004, (d) **g** = 404 and (e) **g** = -404. Dislocations with **b** = [100] are visible in (b), (d) and (e), but they are invisible in (c). Dislocations with **b** = 1/2 <101> are visible in (b) and (c but one of pairs, 1/2[-101] screw dislocations along the [-404] direction or 1/2[101] screw dislocations along the [404] direction is invisible in (d) and (e), respectively. The two-sided arrow on the upper right in (a) indicates approximately the bulk

shear direction in the deformation experiment. The inset in the (a) is the nearest principal zone axis, while the inset of (d) and (e) is the diffraction condition of the WBDF image.

Figure 3. Close-ups of an area in the Fig. 2(c) and the Fig. 2(d), respectively, indicating that (a) two thickness contour fringes are terminated at the extremity of the dislocation and its debris in the WBDF images with **g** = 004 by two white arrowheads and (b) no oscillation contrasts in horizontally elongated dislocation lines of dislocations with **b** = [100] (grey arrowhead), and 1/2[101] (white arrowhead) and 1/2[-101] (residual contrast by **g.b** = 0, black arrowhead). Note: The grey arrowhead in the (a) indicates a different type of dislocation that would be a product of reactions among [100] and 1/2<101> dislocations.

Figure. 4. WBDF-TEM images of the Shockley-type extended dislocation with **b** = 1/2<101>. (a) **g** = -211 and (b) **g** = 013. (a) Fringe contrasts of its associated stacking faults on the (010) plane in the [101] direction are visible in the images (white arrowheads). (**b**) The 1/2[101] dislocations are terminated on the edge of the (010) stacking faults, indicating the partial dislocations (the white arrowhead) was gliding in the (010) plane. The images correspond to the grains of Fig. 2 and Fig. 1(b), respectively. The two-sided arrow on the upper left in (b) indicates approximately the bulk shear direction in the deformation experiment.

Figure 5. Typical dark field TEM images of non-deformed wadsleyite (run M0187 in Kawazoe et al. 2013). (a) **g** = -2-1-1, stacking faults are visible, (b) **g** = 0-80, invisible. Some planar areas in the grain display fringe contrast of stacking faults (indicating white arrowheads) with partial dislocations at the ends, but they are not a glide configuration in contrast to Figure 4b where the (010) stacking fault planes are sub-parallel to a shear direction. The inset in the (b) is the nearest zone axis. The two-sided arrow on the upper right in (a) indicates a potential bulk shear direction.

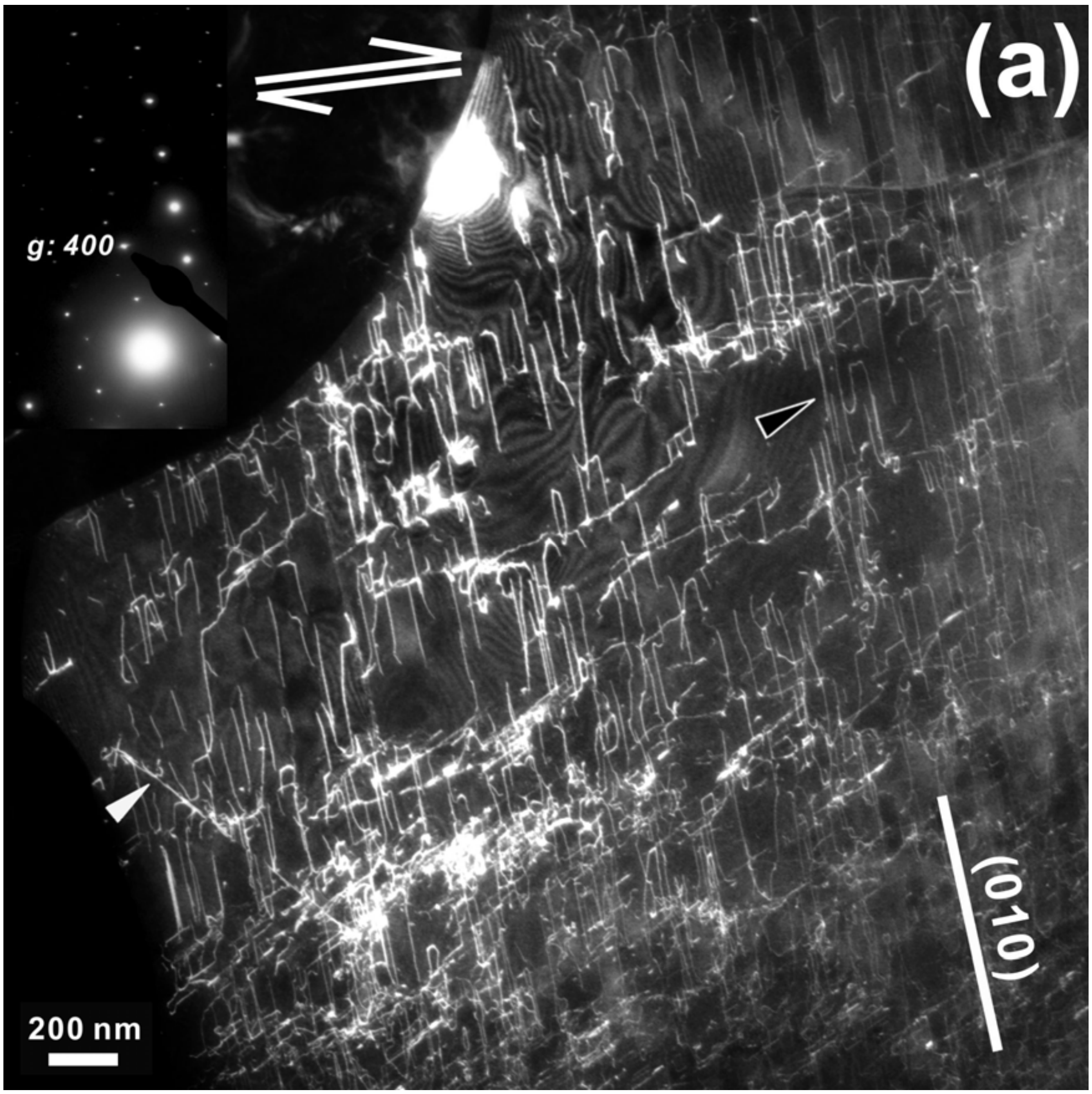
(a)
g: 400
200 nm
(010)

324 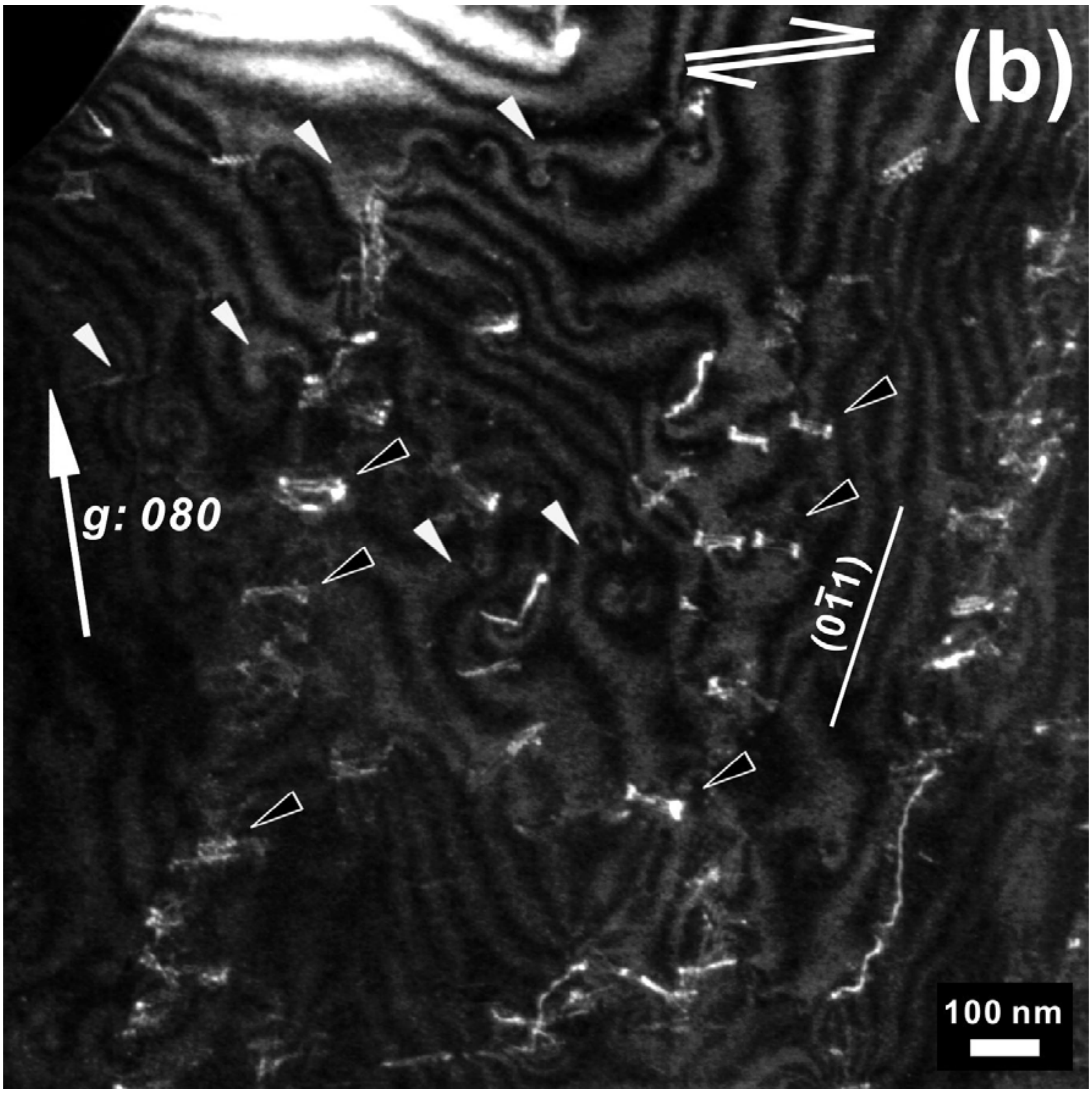

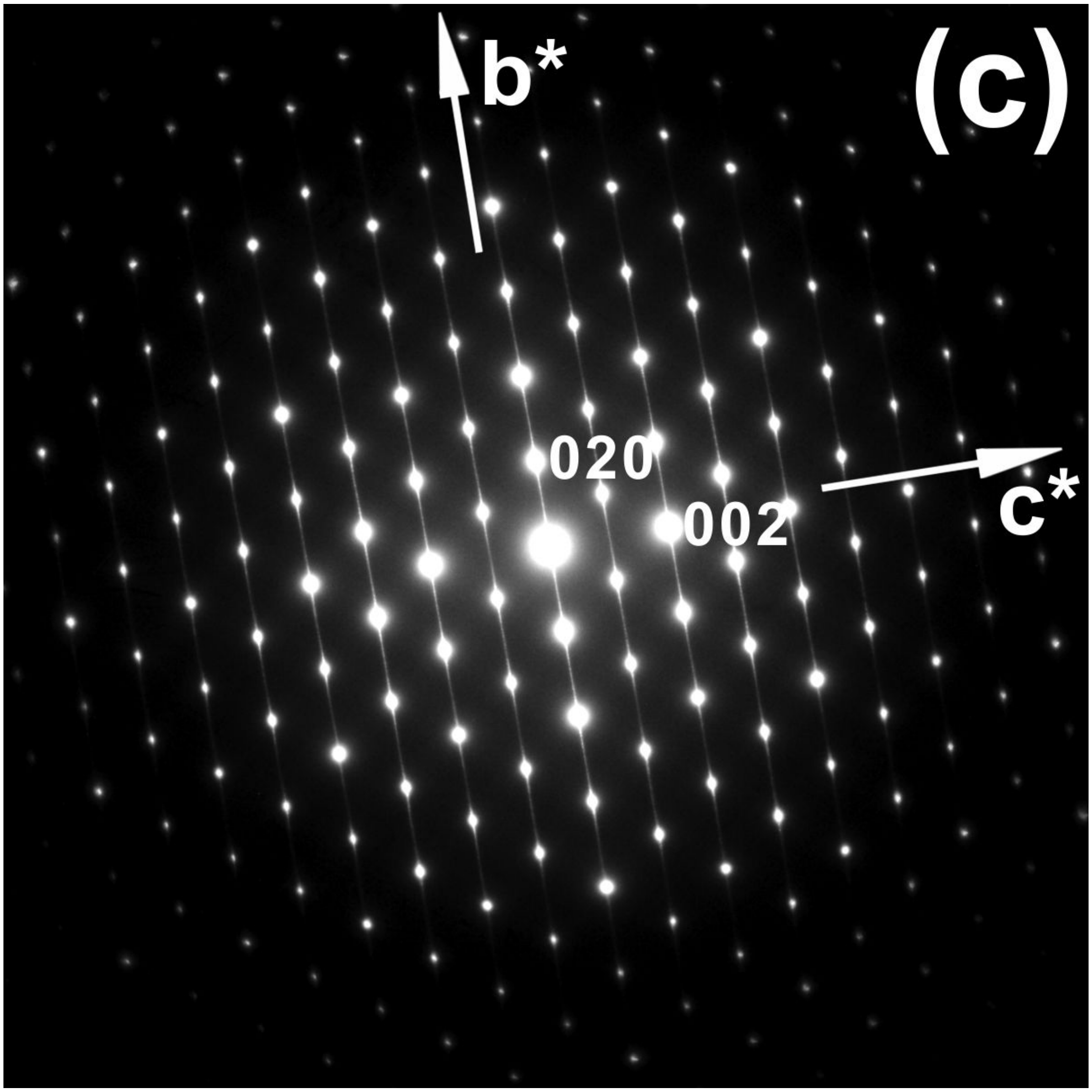

Figure 1. Typical dislocation microstructures of the simple-shear deformed wadsleyite (run M0180 in Kawazoe et al. 2013). (a) Straight, long screw segments of [100] dislocations (black arrowhead) and a few of 1/2[111] dislocations (Lower left, white arrowhead) are visible. (b) Array of 1/2[111] dislocations that have dissociated into several partial dislocations (black arrowheads) are in dislocation bands parallel to the (0-11) plane. The residual contrast of stacking faults on the (010) plane is weakly visible (white arrowheads). The stacking faults on the (010) plane are also indicated by remarkable streak lines along the [010]* direction on the selected

area electron diffraction (SAED) pattern of the nearest zone axis (c). The two-sided arrows on the upper left and upper right in (a) and (b), respectively indicate approximately the bulk shear direction in the deformation experiment.

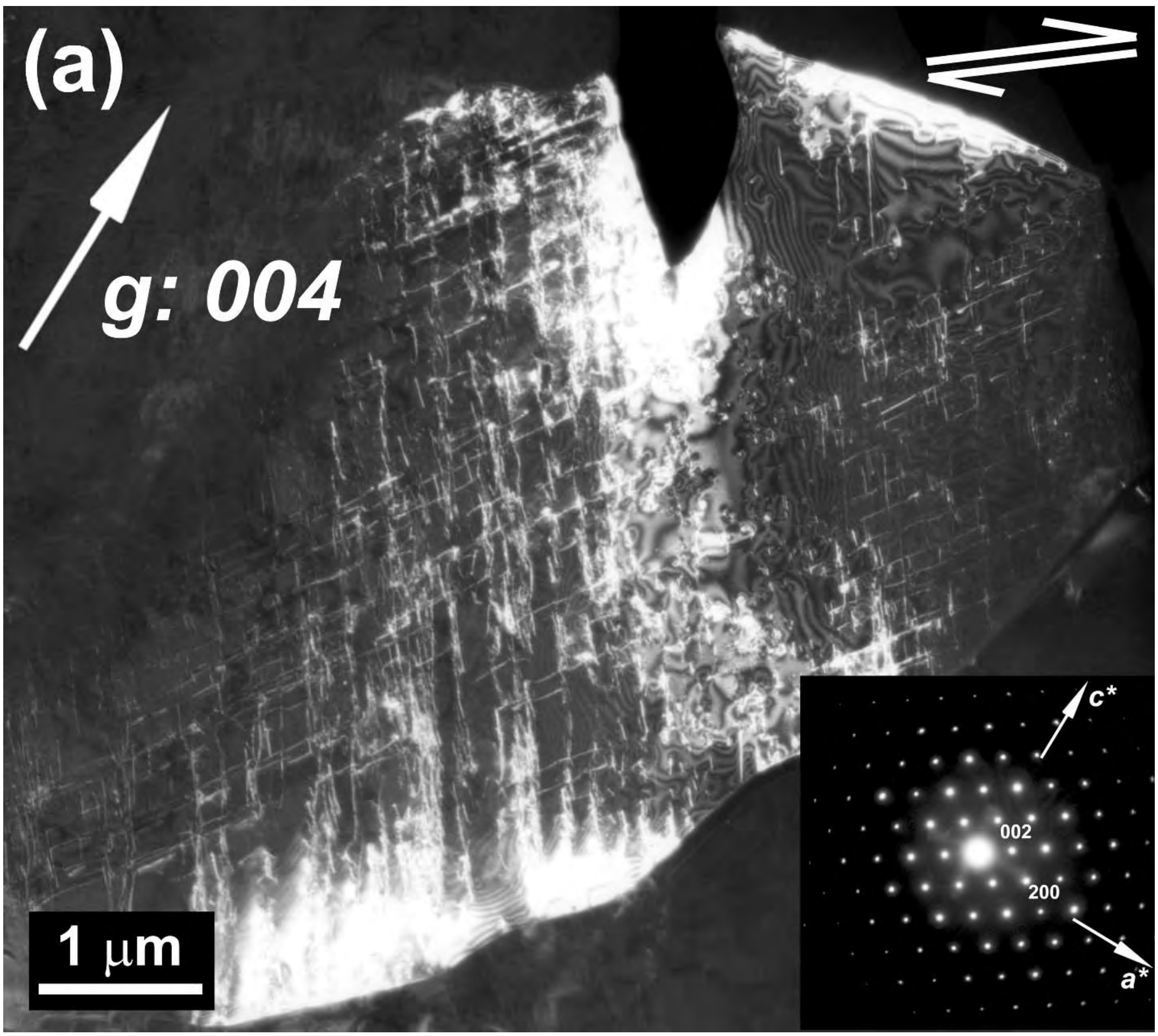

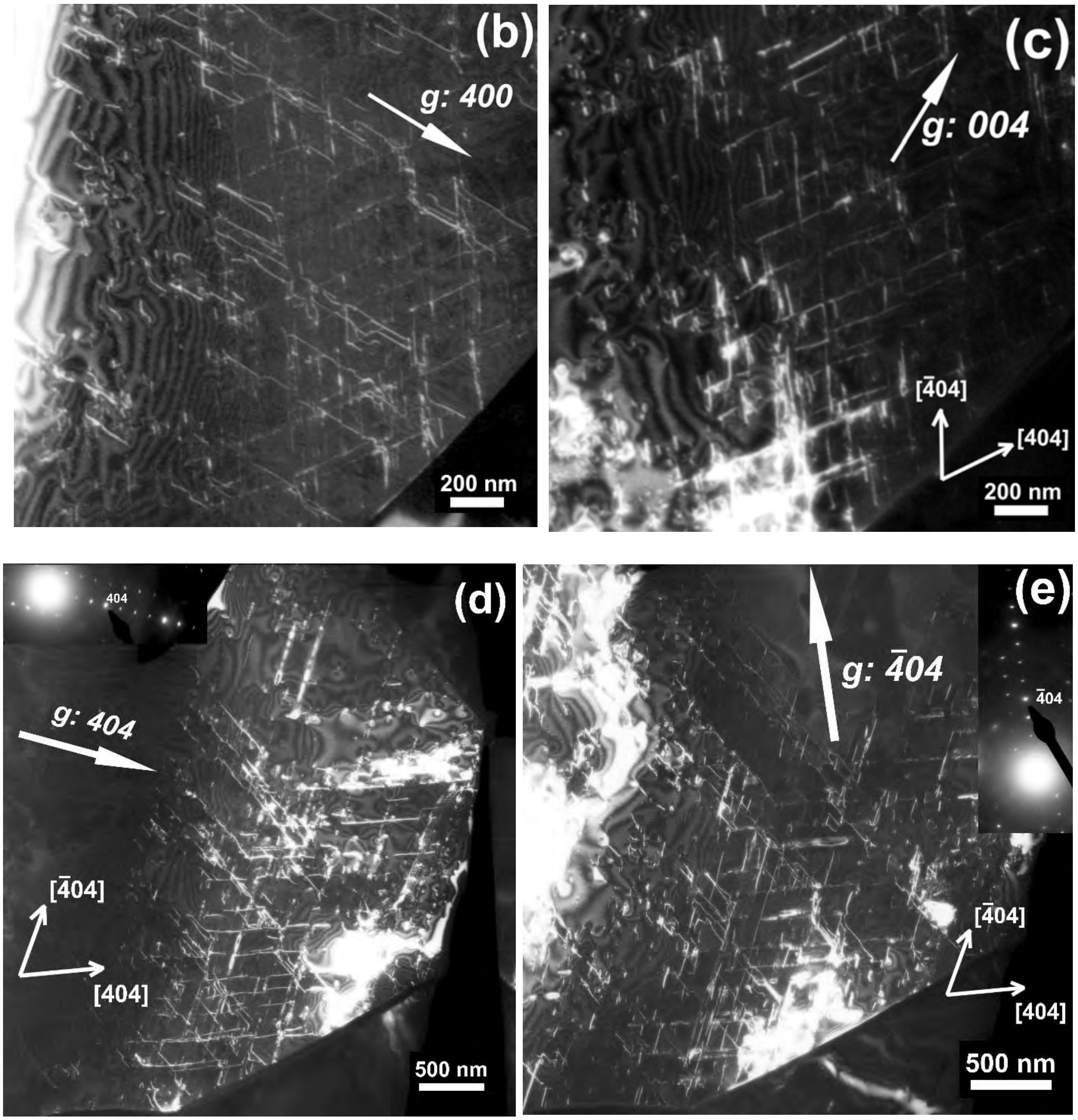

Figure 2. Typical WBDF images of 1/2 <101> dislocations co-activated with [100] dislocations. (a) A whole grain with g = 004, the inset is the nearest principal zone axis. The right half of the grain with (b) g = 400 (c) g = 004, (d) g = 404 and (e) g = -404. Dislocations with b = [100] are visible in (b), (d) and (e), but they are invisible in (c). Dislocations with b = 1/2<101> are visible in (b) and (c), but one of pairs, 1/2[-101] screw dislocations along the [-404] direction or

1/2[101] screw dislocations along the [404] direction is invisible in (d) and (e), respectively. The two-sided arrow on the upper right in (a) indicates approximately the bulk shear direction in the deformation experiment. The inset in the (a) is the nearest principal zone axis, while the inset of (d) and (e) is the diffraction condition of the WBDF image.

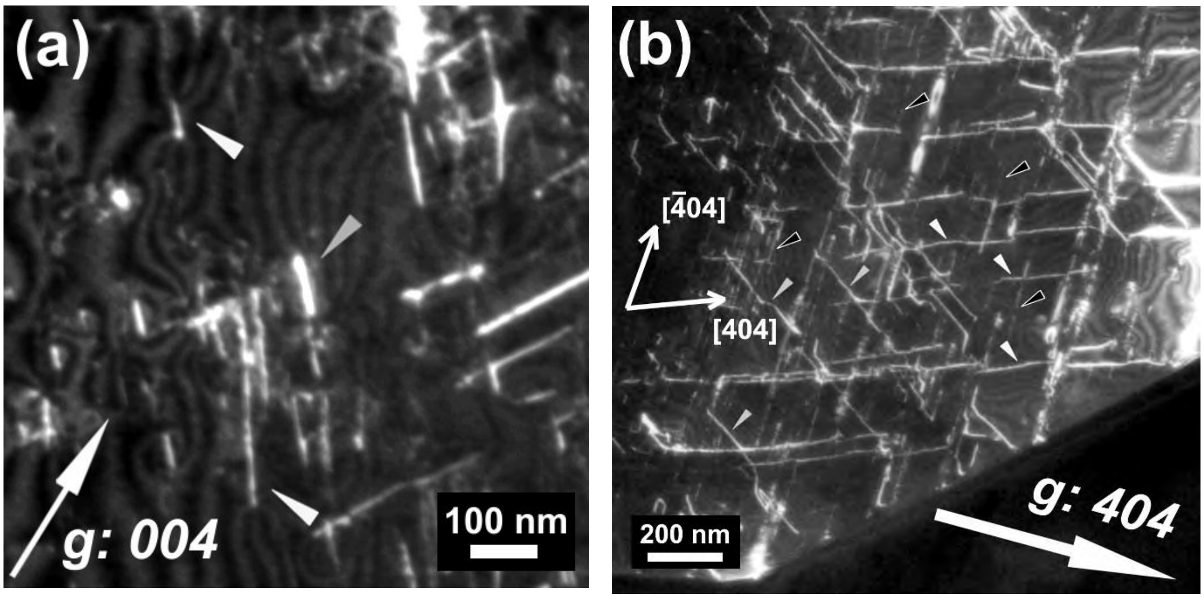

Figure 3. Close-ups of an area in the Fig. 2(c) and the Fig. 2(d), respectively, indicating that (a) two thickness contour fringes are terminated at the extremity of the dislocation and its debris in the WBDF images with **g** = 004 by two white arrowheads and (b) no oscillation contrasts in horizontally elongated dislocation lines of dislocations with **b** = [100] (grey arrowhead), and 1/2[101] (white arrowhead) and 1/2[-101] (residual contrast by **g.b** = 0, black arrowhead). Note: The grey arrowhead in the (a) indicates a different type of dislocation that would be a product of reactions among [100] and 1/2<101> dislocations.

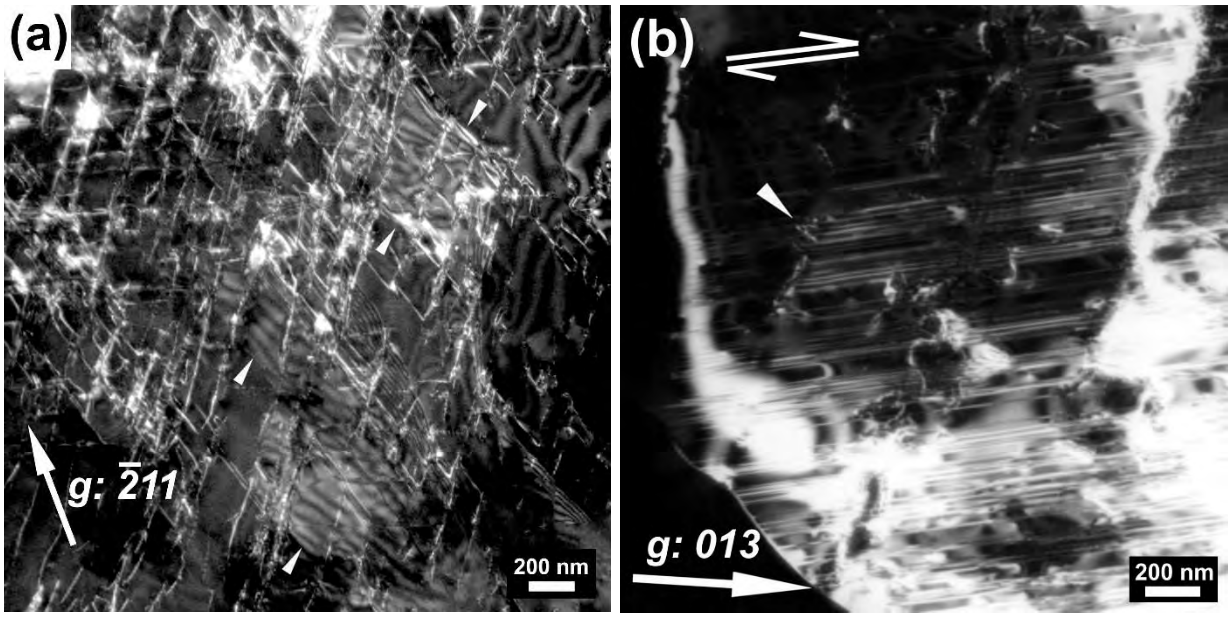

Figure. 4. WBDF-TEM images of the Shockley-type extended dislocation with **b** = 1/2<101>. (a) **g** = -211 and (b) **g** = 013. (a) Fringe contrasts of its associated stacking faults on the (010) plane in the [101] direction are visible in the images (white arrowheads). (b) The 1/2[101] dislocations are terminated on the edge of the (010) staking faults, indicating the partial dislocations (the white arrowhead) was gliding in the (010) plane. The both of images correspond to the grains of Fig. 2 and Fig. 1(b), respectively. The two-sided arrow on the upper left in (b) indicates approximately the bulk shear direction in the deformation experiment.

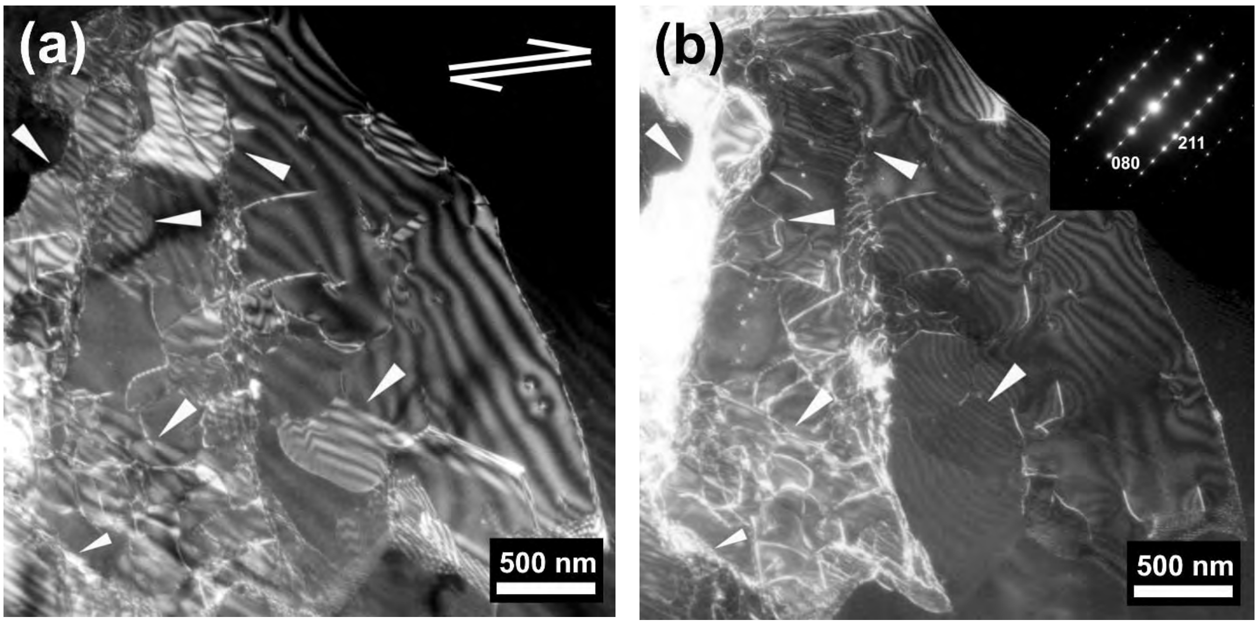

Figure 5. Typical dark field TEM images of non-deformed wadsleyite (run M0187 in Kawazoe et al. 2013). (a) **g** = -2-1-1, stacking faults are visible, (b) **g** = 0-80, invisible. Some planar areas in the grain display fringe contrast of stacking faults (indicating white arrowheads) with partial dislocations at the ends, but they are not a glide configuration in contrast to Figure 4b where the (010) stacking fault planes are sub-parallel to a shear direction. The inset in the (b) is the nearest zone axis. The two-sided arrow on the upper right in (a) indicates a potential bulk shear direction.